Materials Research Proceedings 31 (2023) 755-764 https://doi.org/10.21741/9781644902592-77

A comprehensive analysis of the erosion in a carbon steel boiler tube elbow through the use of 3D mapping of the corroded surface and CFD modelling

Nikolay Bukharin[1,2*], M.A. Farrokhzad[1], Mouhammad El Hassan[3]

[1] The Southern Alberta Institute of Technology, Calgary, Alberta, Canada

[2] Thermofluid Solutions, Calgary, Alberta, Canada

[3] Prince Mohammad Bin Fahd University, Mechanical Engineering Department

* nikolay.bukharin@sait.ca

Keywords: Erosion, Corrosion, Erosion Pattern, CFD, Particulate Matter

Abstract. Erosion corrosion is a common problem that affects boiler tubes, particularly those in power plants and industrial settings where hard water and abrasive particles are present in the flow. These particles can cause physical erosion to the surface of the tubes, which can then lead to further corrosion. This type of corrosion is often accelerated by the high temperatures and pressures present in a boiler system, as well as the presence of oxygen. The combination of physical erosion and chemical corrosion attack can cause significant damage to the tubes, reducing their ability to efficiently transfer heat and potentially leading to system failure. Therefore, it is important to predict rates of erosion to prevent costly and potentially dangerous failures. The focus of this paper is an investigation into the effects of erosion caused by hard water particles on a carbon steel boiler tube elbow (ANSI 16.9). A semi-empirical procedure, which considers properties of the material and flow parameters, is developed for predicting erosion rates. The study revealed that the primary erosion damage occurred on the extrados of the bend. The findings indicated that particles within the flow began to separate from the front wall surface, resulting in significant erosion along the lateral sides. The disappearance of erosion from the front surface of the bend was also consistent with the erosion patters observed on the eroded pipe sample, which was extracted from the line. Moreover, it was demonstrated the presence of two different erosion patterns in the separation region, which matched qualitatively the erosion pattern observed on the sample wall.

Introduction

The phenomenon of erosion, or sometimes, erosion-corrosion in metals is defined as the synergic effect of surface degradation of metals caused by moving corrosive fluids containing erosive undissolved solid particle. Erosion in pipes can be also related to the effect cavitation [1 – 3]. Typically, the high velocity of the fluid containing hard particles induces mechanical wear and abrasion effects, leading to a rapid decay of the metallic surfaces. Additionally, this form of erosion-corrosion effect can be caused by turbulent flow regime at localized site, often due to disruption in the steady flow pattern, such as a flow-directional change at a bend or a mechanical obstacle in a pipe. The complex phenomenon of erosion-corrosion in steels impacts multiple industrial sectors, including but not limited to water injection systems, boilers, oil and gas pipelines, the nuclear power generation sector, slurry transportation (hydrotransport), etc. [4 – 7] Understanding the underlying causes and mechanisms of erosion corrosion is essential for industries that rely on the proper functioning of equipment and infrastructure, as it can help prevent costly and potentially catastrophic accidents.

Various methods are employed to predict the rates, locations, and patterns of erosion-corrosion. In [8] Computational Fluid Dynamics (CFD) simulations of a laminar flow with solid particles

Content from this work may be used under the terms of the Creative Commons Attribution 3.0 license. Any further distribution of this work must maintain attribution to the author(s) and the title of the work, journal citation and DOI. Published under license by Materials Research Forum LLC.

were performed for erosion prediction in 90° elbow. The main goal of this research was to study how different dimensions of sand affect tube corrosion depending on the different aperture of the valve during water flow with solid particles. It was shown that the erosion rate of a pipe elbow when water flows through a valve opening that is conditioned by specific angles (15°, 30°, 45°, and 90°) and injected with particles of varying sizes can exhibit various different scenarios. It has been concluded that a decrease in moving undissolved solid particle size leads to a decrease in erosion rate. Medium-sized particles reduce erosion rate by approximately twice as much as larger particles and ten times as much as smaller particles. In [9], the effect of different parameters such as particles size, stream velocities and elbows diameter on the erosion rate for an elbow in light crude oil-solid flow was studied. Three distinct models were used in this study: continuous flow modeling, Lagrangian particle tracking, and an empirical erosion equation. The parameter ranges evaluated were particle size of 100-500 μm, stream velocities of 3-7 m/s, and elbow diameters of 0.0762-0.1778 m. The numerical results showed that the highest erosion rate increases with bigger particle size and stream velocities, but decreased with increasing elbow bending radius. However, the position of the peak erosion rate in the elbow area was unaffected by these factors. In [10] a new erosion model, which is referred to as SIEM (shear impact energy model), is used to investigate elbow erosion under different working conditions using numerical simulations. The fluid motions are predicted by CFD, and the particle movements are calculated using DEM (discrete element method) in the simulations. Both a one-way coupling method and a two-way coupling method in CFD-DEM are adopted to calculate the gas-solid interaction. Experiments were carried out in [11] with flows comprising of water, air, and sand particles having an average diameter of 300 μm, as well as liquid-sand flows. Wall thickness losses were measured at 63 locations on the outer radius of elbows, across various flow conditions. To explore different flow regimes, Computational Fluid Dynamics (CFD) simulations were conducted using the Euler-Lagrange approach to model turbulence, and the Eulerian Multiphase model to handle multiphase flow scenarios. The Reynolds Stress Model (RSM) was also implemented in the simulations as a turbulence model. The results showed that the maximum erosion increased with increasing mixture velocity. The CFD simulations using the Euler-Lagrange and Euler-Euler-Lagrange approaches accurately predicted the observed maximum erosion rates, erosion locations, and erosion patterns for liquid-sand and dispersed-bubble-sand flows. A numerical study was conducted in [12], to estimate the erosion of solid particles in angle-cutting elbows (ACEs) where there is a flow of gas and solid particles. The simulation models used a combination of the two-way coupled Eulerian-Lagrangian approach and the E/CRC model, along with particle-wall rebound models and a user-defined function in the dispersed phase model. The accuracy of the simulation results was tested by comparing them with previously reported experimental results. The study's outcomes revealed that significant erosion occurs in the downstream section of the concave wall of the ACE, while only minor erosion occurs on the convex wall of the ACE. In [13], a new approach for modeling erosion and corrosion in hydrocarbon pipes using Computational Fluid Dynamics (CFD) has been introduced. This approach was based on high-order Discontinuous Galerkin Spectral Element Method (DGSEM) to approximate the incompressible Navier-Stokes/Cahn-Hilliard model. This technique enables a highly detailed three-dimensional representation of the flow regime, phases distribution, and contact surfaces within the pipe, resulting in precise calculations of erosion and corrosion rates and their distribution over the pipeline surface. The effectiveness of this methodology has been verified with experiments relevant to the oil and gas industry, specifically, by simulating erosion in a one-phase ascending pipe with two elbows and corrosion in a two-phase pipe under various flow regimes. In [14], a process has been developed to forecast erosion rates in pipe elbows and tees, for use in estimating safe operating conditions and velocities during oil and gas production in the presence of sand. The procedure introduces a new concept that enables the calculation of erosion rates for different pipe geometries. It establishes a connection between the

erosion rate and the impact velocity of sand particles on a pipe fitting wall based on empirical observations.

In this paper we are studying the nature of erosion pattern in the sample of carbon steel boiler tube elbow (ASME/ANSI 16.9) using CFD numerical modeling. In the given sample description, it was stated, that the damaged occurred from the solid particles in the hard water flow at the average velocity of 5 m/s. Using numerical calculation in combination with material properties measurements and 3D scanning of the given sample we recreate erosion damage mechanisms. To the far of our knowledge such combination of numeric models and material and geometric measurements in the given geometry is not described in the literature and might be used in development of accurate semi-empirical procedures for erosion prediction and prevention.

CFD Model

Geometry and Mesh

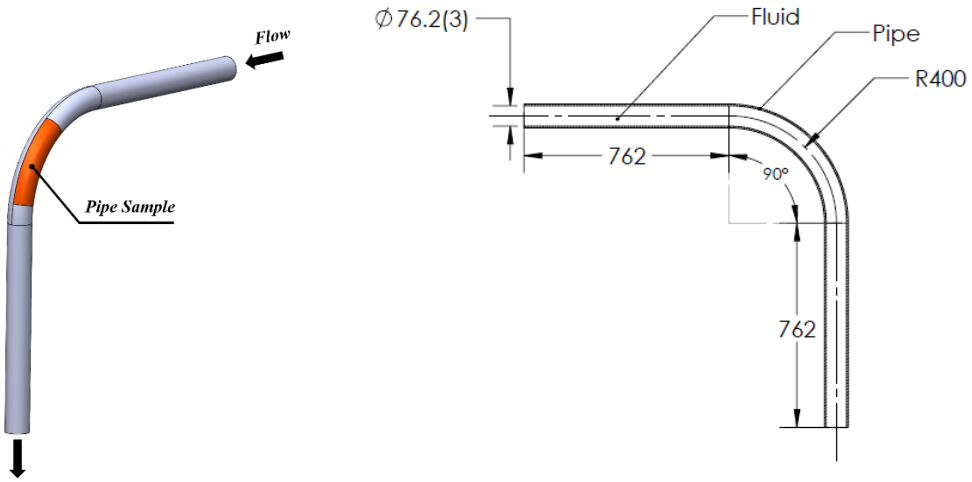

Figure 1. Geometry and location of extracted pipe sample

Figure 1 displays the geometry employed for CFD modeling. Additionally, it shows the flow direction and illustrates the position of the extracted sample from the eroded pipe, which was analyzed in this study.

Figure 2 shows the mesh structure. In the mesh independence analysis, mesh adaptation was used, which utilizes the simulation results to iteratively enhance the mesh structure. This process generates a mesh that is tailored to the specific simulation, with finer mesh elements in regions with high gradients and coarser elements elsewhere (Figure 2d). The total number of elements in the final 3D mesh was 987,201 (when the change in average velocity and pressure between the cycles was less than 1.5%)

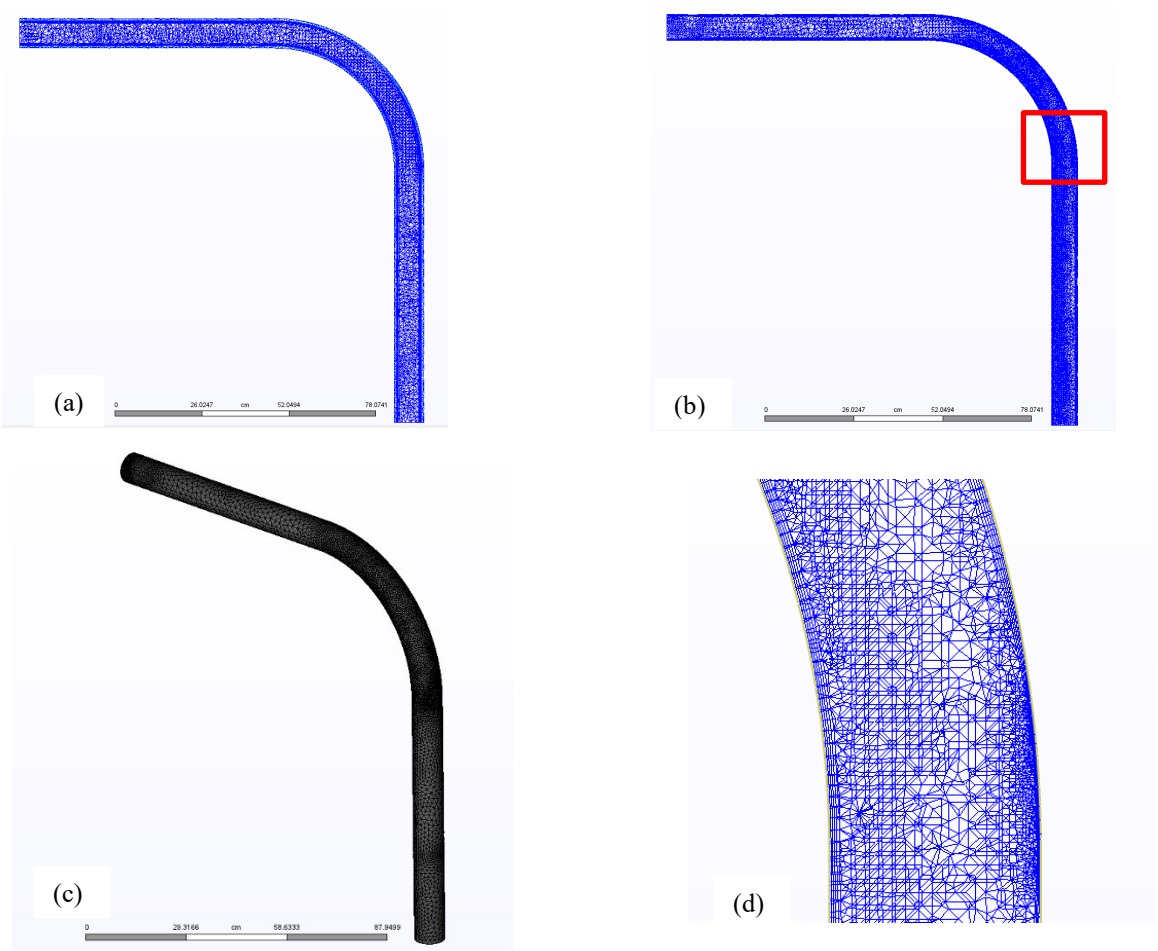

Figure 2. Pipe section. Mesh structure. (a) Initial mesh, (b) Final refined mesh based on mesh adaptation (red square shows zoomed region in (d)), (c) 3D mesh structure, (d) Zoomed mesh region

Turbulence model and boundary conditions.

For the CFD analysis a RANS (Reynolds-averaged Navier–Stokes) RNG k–ε turbulence model was employed. This model was developed using re-normalization group (RNG) methods to re-normalize the Navier–Stokes equations, thereby accounting for the impact of smaller scales in the flow [15],[16]. The RNG k-ε turbulence model is analogous in structure to the standard k-ε model and yields an analytical derivation of the model constants that differ from those in the standard model. Additionally, it introduces new terms in the transport equations for k and ε, allowing for more accurate predictions. The reduced dependence on empirical data and the incorporation of these additional terms make the RNG k-ε model more accurate for a wider range of flows than the standard k-ε model.

The eddy viscosity and eddy conductivity are calculated as follows:

$$\mu_t = C_\mu \rho \frac{K^2}{\varepsilon}\,;\, k_t = \frac{\mu_t C_p}{\sigma_t}$$

where σ_t is a turbulent Prandt number, usually taken to be 1.0 and C_μ is an empirical constant. The momentum equations are transformed to wave-number space and re-normalization group

Materials Research Proceedings 31 (2023) 755-764 https://doi.org/10.21741/9781644902592-77

theory is used to derive the equations for calculating eddy viscosity. The equation used for K (Turbulent Kinetic Energy) is:

$$\rho\frac{\partial K}{\partial t}+\rho U\frac{\partial K}{\partial x}+\rho V\frac{\partial K}{\partial y}+\rho W\frac{\partial K}{\partial z}=\frac{\partial}{\partial x}\left[\left(\frac{\mu_t}{\sigma_K}+\mu\right)\frac{\partial K}{\partial x}\right]+\frac{\partial}{\partial y}\left[\left(\frac{\mu_t}{\sigma_K}+\mu\right)\frac{\partial K}{\partial y}\right]+\frac{\partial}{\partial z}\left[\left(\frac{\mu_t}{\sigma_K}+\mu\right)\frac{\partial K}{\partial z}\right]-\rho\varepsilon+\mu_t\left[2\left(\frac{\partial U}{\partial x}\right)^2+2\left(\frac{\partial V}{\partial y}\right)^2+2\left(\frac{\partial W}{\partial z}\right)^2+\left(\frac{\partial U}{\partial y}+\frac{\partial V}{\partial x}\right)^2+\left(\frac{\partial U}{\partial z}+\frac{\partial W}{\partial x}\right)^2+\left(\frac{\partial V}{\partial z}+\frac{\partial W}{\partial y}\right)^2\right]$$

The equation for ε (Turbulent Energy Dissipation)

$$\rho\frac{\partial \varepsilon}{\partial t}+\rho U\frac{\partial \varepsilon}{\partial x}+\rho V\frac{\partial \varepsilon}{\partial y}+\rho W\frac{\partial \varepsilon}{\partial z}=\frac{\partial}{\partial x}\left[\left(\frac{\mu_t}{\sigma_\varepsilon}+\mu\right)\frac{\partial \varepsilon}{\partial x}\right]+\frac{\partial}{\partial y}\left[\left(\frac{\mu_t}{\sigma_\varepsilon}+\mu\right)\frac{\partial \varepsilon}{\partial y}\right]+\frac{\partial}{\partial z}\left[\left(\frac{\mu_t}{\sigma_\varepsilon}+\mu\right)\frac{\partial \varepsilon}{\partial z}\right]-C_2\rho\frac{\varepsilon^2}{K}+C_1\mu_t\frac{\varepsilon}{K}\left[2\left(\frac{\partial U}{\partial x}\right)^2+2\left(\frac{\partial V}{\partial y}\right)^2+2\left(\frac{\partial W}{\partial z}\right)^2+\left(\frac{\partial U}{\partial y}+\frac{\partial V}{\partial x}\right)^2+\left(\frac{\partial U}{\partial z}+\frac{\partial W}{\partial x}\right)^2+\left(\frac{\partial V}{\partial z}+\frac{\partial W}{\partial y}\right)^2\right]$$

C_1 is calculated using the following expression:

$$C_1=C_0-\frac{\eta\left(1-\frac{\eta}{\eta_0}\right)}{1+\beta\eta^3}$$

Where η is defined as:

$$\eta=\frac{\sqrt{G}K}{\varepsilon}$$

$$G=2\left[\left(\frac{\partial U}{\partial x}\right)^2+\left(\frac{\partial V}{\partial y}\right)^2+\left(\frac{\partial W}{\partial z}\right)^2\right]+\left(\frac{\partial U}{\partial y}+\frac{\partial V}{\partial x}\right)^2+\left(\frac{\partial U}{\partial z}+\frac{\partial W}{\partial x}\right)^2+\left(\frac{\partial V}{\partial z}+\frac{\partial W}{\partial y}\right)^2$$

Other constants were adjusted directly in the solver.

We used velocity boundary condition on the inlet of the pipe and “Unknown” boundary condition on the outlet of the pipe. The Unknown boundary condition is a mixed Neumann-Dirichlet-type (specified value) boundary condition applied to the pressure variable. It is implemented into the solution in a two-part process. During the matrix solution of the pressure equation, nodes assigned an Unknown boundary condition are treated as fixed or specified (Dirichlet) and after the matrix solution, the values on these nodes are re-calculated as the average of the neighboring values, effectively enforcing a zero gradient (Neumann) condition on the pressure equation (Figure 3).

Autodesk CFD software package was used for all numerical calculations in the present study.

Materials Research Proceedings 31 (2023) 755-764 https://doi.org/10.21741/9781644902592-77

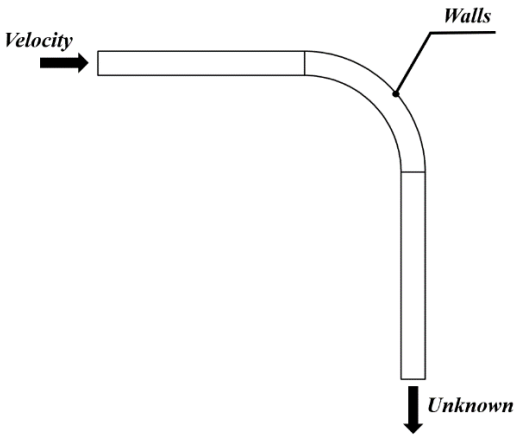

Figure 3. Boundary conditions

Temperature affects were not studied in this paper and temperature was considered 20ºC within computation domain.

Erosion model

Lagrangian particle tracking with the Edwards Model [17] is used to compute erosion. A low particle concentration assumption (not a slurry erosion model) is employed, and results are presented as a scalar result quantity. This facilitates design comparison, and removes the guesswork from interpreting erosion predictions. The erosion model uses angle of attack bounce data and the Brinell material hardness to compute the material volume removal rate. This approach qualitatively identifies areas subject to erosion. It illustrates the relationship between the flow and erosion trends, which can lead to erosion reduction through design improvements. Spherical particles were considered in this study with the radius of 0.36mm and density of 2750 kg/m^3. In order to accurately measure all geometrical parameters of the given sample and to identify its exact location in the elbow it was 3D scanned using the high-end HandySCAN 3D (BLACK Series) 3D scanner with the accuracy of 0.025mm and 0.1mm of mesh resolution. A pipe sample and a scanned 3D image with hardness measurements locations are shown in Figure 4.

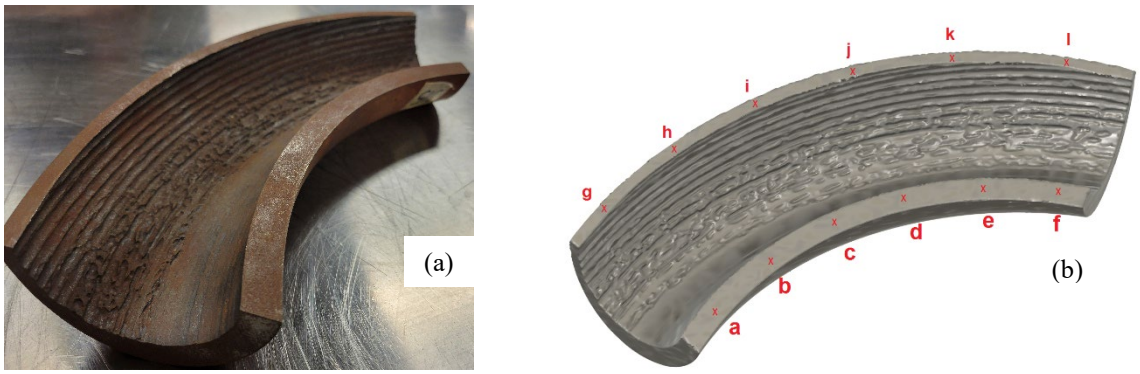

Figure 4. (a) Eroded pipe, (b) 3D Scan of eroded pipe with shown hardness measurements locations.

In order to include the surface hardness of the bend interior in the erosion simulation models, hardness measurements (indentations) were conducted using Rockwell Hardness Testing method

Materials Research Proceedings 31 (2023) 755-764 https://doi.org/10.21741/9781644902592-77

(HRB). 36 indentations were placed alongside the bend to represent its hardness map. 18 of these hardness indentations were placed in group of three at 15° angle increments at the bend's intrados cross-section and their average values are shown in Table 1. The other 18 indentation were placed at the extrados cross-section of the bend (in group of three and at 15° angle increments as well) and their average per location is also shown in Table 1.

For the Rockwell test, the test was carried out with a Mitutoyo, Model ARK-600 (Japan) Hardness Tester using 1/16" diameter tungsten carbide (WC). The applied load was set at 100 kg for duration of 8 seconds.

The higher hardness values at the extrados were expected and are believed to be the result of work-hardening occurred during the bend process from pipe to elbow.

It shall be noted that the CFD model used in this study uses Brinell hardness values, however due to the size limitations of elbow thickness versus the size of Brinell hardness indenter (10 mm), applying the Brinell hardness measurements was not possible. Therefore, the hardness tests were conducted using Rockwell hardness tests (smaller indenter) and for the purpose of CFD modeling, the Rockwell hardness values (HRB) were converted to Brinell hardness (HB) values. The average value (226) was used as one of the inputs in CFD model.

Table 1: Rockwell-Ball (HRB) Hardness Measurements, the values shown in the brackets are the Brinell Hardness (HB)values calculated from hardness conversion tables.

		Intrados		Extrados
15°	a	92.3 (eq. 194HB)	g	97.1 (eq. 221 HB)
30°	b	93.9 (eq. 203 HB)	h	98.0 (eq. 227 HB)
45°	c	93.6 (eq. 200 HB)	i	98.4 (eq. 230 HB)
60°	d	94.8 (eq. 208 HB)	j	98.4 (eq. 230 HB)
75°	e	91.3 (eq. 189 HB)	k	98.2 (eq. 229 HB)
90°	f	88.7 (eq. 177 HB)	l	96.6 (eq. 218 HB)

CFD Results

In order to investigate the relationship between the flow dynamics and the erosion pattern inside the bend, the velocity distribution and the erosion rate are investigated using the CFD results. Figure 5 shows the velocity field inside the pipe in the midplane section and erosion on the front wall of a bend. As the flow approaches the bend, it becomes fully developed and the solid particles gain enough momentum to deviate from the intrados due to the sudden change in flow direction. This results in the solid particles collide directly with the extrados. Particles on extrados are being dragged along the wall with the flow, producing erosion. When they reach the mark shown in Figure 5, particles start to separate from pipe surface and continues to travel along the wall on the lateral sides (Figure 6). It can be also seen (Figure 5) that the velocity distribution is not uniform across the bend and that the velocity magnitudes are higher on the external wall which correlates well with the erosion pattern. The flow begins to gradually recover downstream of the bend to almost fully re-establish at the pipe exit.

Materials Research Proceedings 31 (2023) 755-764 https://doi.org/10.21741/9781644902592-77

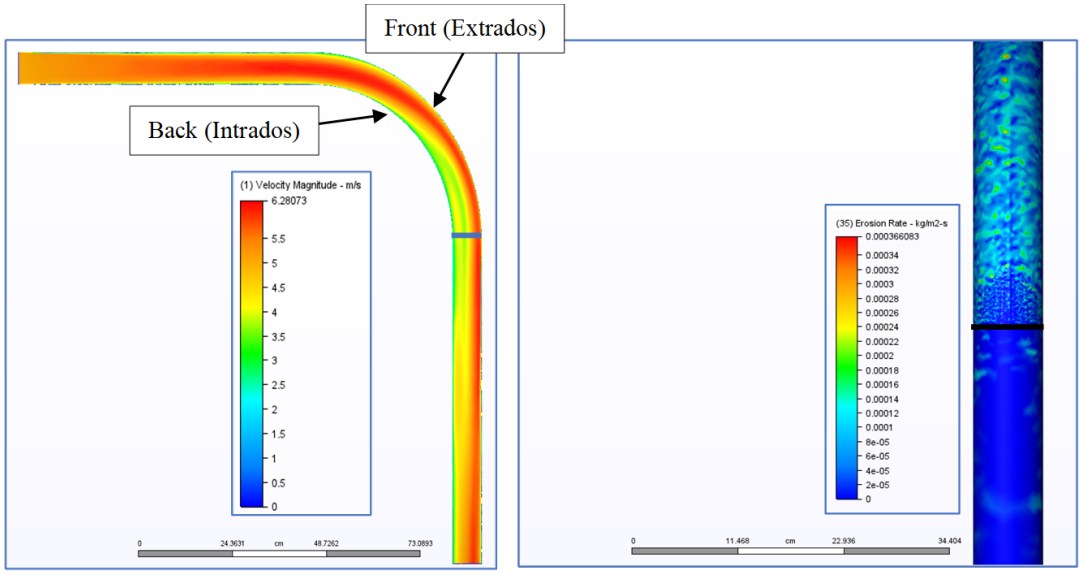

Figure 5 (a) Velocity magnitude in the midsection view, (b) Front erosion pattern.

Figure 6b shows two types of erosion pattern that are formed in the particle separation region. The major mass of particles moves to the lateral sides producing same pattern as prior to separation on extrados and separating particles on front produce less erosion and generate more regular pattern. A similar behavior can be observed on the pipe sample (Figure 4), as well as absence of erosion on intrados (Figure 6c).

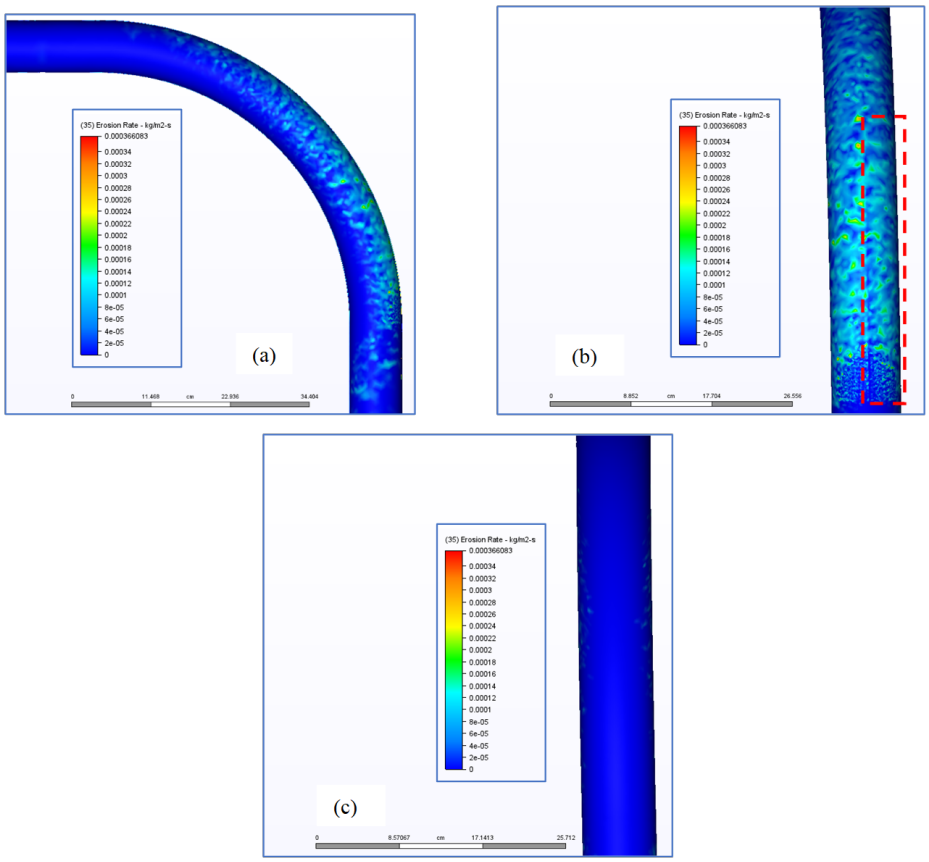

Figure 6. Elbow erosion. (a) Side view, (b) Magnified front view, sample location is marked with red, (c) Intrados

Conclusion

In this study, a numerical analysis of 90 degrees carbon steel boiler tube elbow (ASME/ANSI 16.9), combined with geometrical and material hardness measurements, was conducted. It was shown that the main erosion damage was produced along the extrados of the bend. It was shown that particles in the flow at some point start to separate from the front wall surface and start to travel along the lateral sides producing significant erosion in those regions. It was also found that erosion disappears from the front surface of the bend. These results corroborated well with the experimental results. It was also demonstrated that in the separation region two different erosion pattern existed which also correlates with erosion pattern observed on the sample wall. Finally, it should be noted that the straight lines erosion pattern is not completely clear and needs additional investigation.

References

[1] Farrokhzad, M. A., Saha, G.C., Khan, T.I. (2013) Wear performance of co-electrodeposited cermet coatings, Surface and Coatings Technology 235(1-2):75–85 https://doi.org/10.1016/j.surfcoat.2013.07.015

[2] Farrokhzad, M. A., Saha, G.C., Khan, T.I. (2014) Three-body wear performance of co-electrodeposited cermet coatings, Wear Volume 313(Issues 1-2):34–42, https://doi.org/10.1016/j.wear.2014.02.013

[3] El Hassan, M.; Bukharin, N.; Al-Kouz, W.; Zhang, J.-W.; Li, W.-F. (2021). A Review on the Erosion Mechanism in Cavitating Jets and Their Industrial Applications. Appl. Sci., 11, 3166. https://doi.org/10.3390/app11073166

[4] M.C. Roco, G.R. Addie, (1987). Erosion wear in slurry pumps and pipes, Powder Technology, 50, 1, 35-46, ISSN 0032-5910, https://doi.org/10.1016/0032-5910(87)80081-5

[5] H., Wael, (2012). Flow Accelerated Corrosion in Nuclear Power Plants, Nuclear Power - Practical Aspects, InTech, https://doi.org/10.5772/51346

[6] P. C. Okonkwo, A. M. Mohamed, (2014). Erosion-corrosion in oil and gas industry: a review, International Journal of Metallurgical & Materials Science and Engineering, 4, 3, 7-28

[7] A.V. Levy, (1993). The erosion-corrosion of tubing steels in combustion boiler environments, Corrosion Science, 35, 5–8,1035-1043, ISSN 0010-938X, https://doi.org/10.1016/0010-938X(93)90322-8

[8] M. Amara, B.G.N. Muthanna, M. Tahar Abbes, M. Hadj Meliani, (2018). Effect of sand particles on the Erosion-corrosion for a different locations of carbon steel pipe elbow, Procedia Structural Integrity, Volume 13, Pages 2137-2142, ISSN 2452-3216, https://doi.org/10.1016/j.prostr.2018.12.151

[9] M. A. H. Yusof, Z. Zakaria, A. Supee, M. Z. M. Yusop, N. B. Haladin, (2019). Prediction of Erosion Rate in Elbows for Liquid-Solid Flow via Computational Fluid Dynamics (CFD), Applications of Modelling and Simulation, 3(1), 28-38

[10] L. Xu, Q. Zhang, J. Zheng, Y. Zhao, (2016). Numerical prediction of erosion in elbow based on CFD-DEM simulation, Powder Technology, Volume 302, Pages 236-246, ISSN 0032-5910, https://doi.org/10.1016/j.powtec.2016.08.050

[11] T. A. Sedrez, S. A. Shirazi, Y. R. Rajkumar, K. Sambath, H. J. Subramani, (2019). Experiments and CFD simulations of erosion of a 90° elbow in liquid-dominated liquid-solid and dispersed-bubble-solid flows, Wear, Volumes 426–427, Part A, Pages 570-580, ISSN 0043-1648, https://doi.org/10.1016/j.wear.2019.01.015

[12] R. Liu, W. Yu, M. Liu, (2023). Numerical prediction of solid particle erosion in angle-cutting elbows with gas–solid flow, Proceedings of the Institution of Mechanical Engineers, Part C: Journal of Mechanical Engineering Science, 06-320, 237, 2, https://doi.org/10.1177/09544062221121986

[13] Redondo, C., Chávez–Modena, M., Manzanero, J., Rubio, G., Valero, E., Gómez–Álvarez, S., & Rivero–Jiménez, A. (2021). CFD–based erosion and corrosion modeling in pipelines using a high–order discontinuous Galerkin multiphase solver. Wear, 478-479, 203882, https://doi.org/10.1016/j.wear.2021.203882

[14] Shirazi, S. A., Shadley, J. R., McLaury, B. S., & Rybicki, E. F. (1995). A Procedure to Predict Solid Particle Erosion in Elbows and Tees, Journal of Pressure Vessel Technology, 117(1), 45. https://doi.org/10.1115/1.2842089

[15] Yakhot, V., Orszag, S.A., Thangam, S., Gatski, T.B., Speziale, C.G., (1992), Development of turbulence models for shear flows by a double expansion technique., Phys. Fluids A, 4, 1510–1520, https://doi.org/10.1063/1.858424

[16] Omelyanyuk M, Pakhlyan I, Bukharin N, El Hassan M. (2021). Reduction of Energy Consumption for Water Wells Rehabilitation. Technology Optimization. Fluids., 6(12):444. https://doi.org/10.3390/fluids6120444

[17] Edwards, J. K., McLaury B. S., Shirazi S. A. (2000). Evaluation of Alternative Pipe Bend Fittings in Erosive Service. Proceedings of FEDSM 2000. ASME Fluid Engineering Division Summer Meeting: 959-966